Structures of bovine and human papillomaviruses

Analysis by cryoelectron microscopy and three-dimensional image reconstruction

Timothy S. Baker,* William W. Newcomb,‡ Norman H. Olson,* Lex M. Cowsert,§ Carl Olson,‖ and Jay C. Brown‡

*Department of Biological Sciences, Purdue University, West Lafayette, Indiana 47907; ‡Department of Microbiology and Cancer Center, University of Virginia School of Medicine, Charlottesville, Virginia 22908; §Isis Pharmaceuticals, Carlsbad Research Center, Carlsbad, California 92008; and ‖Department of Veterinary Science, University of Wisconsin, Madison, Wisconsin 53706

ABSTRACT The structures of bovine papillomavirus type 1 (BPV-1) and human papillomavirus type 1 (HPV-1) were determined at 2.5 nm resolution by cryoelectron microscopy and three dimensional image reconstruction techniques. As expected, the reconstructions showed that both viruses consist of a $T = 7$ icosahedral capsid (~60 nm in diameter) which surrounds a nucleohistone core. The capsid morphologies of the two viruses are nearly indistinguishable. Each capsid consists of a shell layer (~2 nm thick) of nearly continuous density from which capsomers project radially to a maximum height of ~5.8 nm. The five-coordinate (pentavalent) and six-coordinate (hexavalent) capsomers both exhibit distinct five-fold axial symmetry as was observed for SV40 and polyoma viruses. Thus, both genera (papilloma and polyoma) of the papovavirus family have now been shown to have the characteristic "all-pentamer" capsid construction. BPV-1 and HPV-1 capsomers consist of a thick (8.6 nm diameter) trunk that broadens distally to form a regular five-pointed, star-shaped head, and proximally to create the shell layer where capsomers associate. A cylindrical channel (~2.8 nm diameter) extends along the axis of each capsomer from the interior of the virus to a point approximately half way to the capsomer surface. Computationally sectioned views of individual capsomers displayed at decreasing radii show that each of the five capsomer subunits (in both pentavalent and hexavalent capsomers) makes a pronounced (30°) left-handed twist just above the outer surface of the capsid shell. Similar views of the reconstructions also clarify the morphology of intercapsomer contacts. For example, they show how hexavalent capsomers coordinate six neighboring capsomers despite the fact that they contain only five subunits. The system of intercapsomer contacts is indistinguishable in BPV-1 and HPV-1, but quite different from that reported for polyoma virus capsids assembled in vitro from the major capsid protein, VP1 (D. M. Salunke, D. L. D. Caspar, and R. L. Garcea. 1989. *Biophys. J.* 56:887–900). Thus, because both polyoma and papilloma viruses have all-pentamer capsids, it appears that intracapsomer subunit–subunit interactions which stabilize pentameric capsomers are better preserved evolutionarily than those involved in capsomer–capsomer contacts.

INTRODUCTION

The papovavirus family consists of two genera, the polyomaviruses and the papillomaviruses, and both include human pathogens. JC and BK are examples of pathogenic polyomaviruses; these cause progressive multifocal leukoencephalopathy and a hemorrhagic cystitis, respectively. Among the 58 or more types of human papillomaviruses are viruses that cause a variety of skin warts and neoplasms (Shah, 1990; Shah and Howley, 1990; Walker and Frisque, 1986; Pfister, 1987); many vertebrate animal species can be infected by species–specific papillomaviruses that cause comparable skin disorders.

Papovaviruses contain a single, circular molecule of dsDNA (~5,200 bp for polyoma and ~8,000 bp for papilloma) associated with histones (or histonelike proteins) inside an unenveloped, icosahedral capsid (Baker and Rayment, 1987; Pfister, 1987; Brady and Salzman, 1986; Howley, 1990). In both genera, virion capsids consist of 72 capsomers arranged on a $T = 7$ icosahedral lattice, with all papovaviruses except cottontail rabbit papillomavirus displaying a *d* (right) hand skew lattice (Finch and Klug, 1965). For two members of the polyoma genus, polyoma virus and SV40, capsid structures have been determined at sufficient resolution by x-ray diffraction (Rayment et al., 1982) and electron microscopy (Baker et al., 1988, 1989) to demonstrate that all capsomers have distinct fivefold symmetry and are therefore most likely to be pentamers of the major capsid protein. This result, which seemed surprising at first because bonding specificity was not conserved (Caspar and Klug, 1962; Eisenberg, 1982; Klug, 1983), indicates that capsomers must exist in two states, one capable of making contact with six neighbors as observed in the 60 hexavalent capsomers and the other with five as found in the 12 pentavalent capsomers (Pentavalent capsomers and hexavalent capsomers will hereinafter be identified as "5-capsomers" and "6-capsomers", respectively.) (Rayment et al., 1982; Salunke et al., 1989). Salunke et al. (1989) have clarified how this occurs in the case of in vitro-assembled polyoma capsids consisting of cloned VP1. Pentameric capsomers have also been shown to be the structural elements of at least two types of tube assemblies recovered from cells infected with polyoma virus (Baker et al., 1983) and of various

0006-3495/91/12/1445/12 $2.00

structures, including empty capsids, formed in vitro from purified polyoma VP1 (Salunke et al., 1986; Salunke et al., 1989).

In view of the polyoma and SV40 structure determinations and the known similarities among papovaviruses, it was attractive to assume that the papillomaviruses might have similar "all-pentamer" capsids. Until now, however, no papillomavirus structure has been determined at sufficient resolution to permit a definitive assignment (Klug and Finch, 1965; Crowther and Amos, 1972). The larger capsid diameter (~ 60 nm cf ~ 50 nm) and greater mass of the major capsid protein (M_r ~ 55,000 for L1 cf M_r ~ 42,000 for VP1) in papilloma compared to polyoma viruses have suggested that there may be significant differences in the capsids of the two types of viruses.

Here we describe the results of studies that were undertaken to define the capsomer symmetry and morphology in two representative papillomaviruses, bovine papillomavirus type 1 (BPV-1) and human papillomavirus type 1 (HPV-1). Beginning with electron micrographs of virions preserved in the frozen-hydrated state (Adrian et al., 1984; Stewart and Vigers, 1986; Chiu, 1986), three-dimensional reconstructions of the two viruses were computed using a modified "common lines" method (Crowther et al., 1970*a*; Crowther, 1971; Fuller, 1987; Baker et al., 1988, 1989). Reconstructions were calculated at a resolution (2.5 nm) sufficient to define the capsomer symmetry, to reveal differences between 5-capsomer and 6-capsomer morphology, and to provide basic information about the nature of intercapsomer contacts. The results are consistent with and amplify those obtained from an earlier reconstruction of negatively-stained HPV (Crowther and Amos, 1972).

MATERIALS AND METHODS

Virus isolation and characterization

BPV-1 was obtained from a calf fibropapilloma (isolate 307) in 1965 and passaged in vivo in 1986 (calf 922). Papillomas resulting from this passage were excised and stored at 2–3°C in phosphate-buffered saline (PBS) containing 50% glycerol. Virus was purified from epithelial tissue by the method of Cowsert et al. (1987). After CsCl banding, the virus was dialyzed against PBS at a concentration of ~3 mg/ml and examined in the electron microscope within 48 h. SDS-polyacrylamide gel analysis (Newcomb and Brown, 1988) of the purified virus showed a band (M_r 55,000) corresponding to the major capsid protein (L1) and three bands corresponding to cellular histones. DNA–DNA hybridization experiments (Lancaster and Olson, 1978) demonstrated that this virus corresponded to BPV-1.

HPV-1 was isolated from human plantar warts collected in the Washington, D.C. metropolitan area. Warts containing HPV-1 were identified by immunofluorescence of frozen sections using a papillomavirus genus-specific (1H8) monoclonal antibody (Cowsert et al., 1988) and an HPV-1 type-specific polyclonal antiserum (A. B. Jenson and L. M. Cowsert, unpublished observations). Virus was purified from HPV-1-containing warts as described above for BPV-1 (Cowsert et al., 1987). Following dialysis against PBS, DNA was extracted from purified virions, digested with BamHI, BglII, or PvuII, and shown by agarose gel electrophoresis to yield digestion products consistent with identification of the virus as HPV-1 (Danos et al., 1982). Purified polyoma virus was the gift of W. Murakami (Brandeis University).

Cryoelectron microscopy

Cryoelectron microscopy was performed as previously described (Baker et al., 1990; Yeager et al., 1990) beginning with BPV-1 or HPV-1 specimens dissolved in 0.02 M Tris-HCl pH 7.4, 0.25 M NaCl at a concentration of 1.0–1.5 mg/ml. Micrographs were recorded as focal pairs, the first at ~1.0 μm underfocus and the second at ~1.6 μm; reconstructions were calculated from micrographs recorded closer to focus (i.e., ~1.0 μm underfocus). All micrographs were recorded at an irradiation level of 800–1,000 electrons/nm^2. The magnification of the BPV-1 micrograph (35,600×) was determined with polyoma virus as an internal standard (Belnap, Olson and Baker, unpublished observation); in the case of HPV-1 the magnification (36,250×) was estimated by comparing radial density plots of the HPV-1 and BPV-1 reconstructions.

Image analysis and three dimensional reconstruction

Images of individual virions employed in the reconstructions were chosen at random from regions of micrographs (such as that shown in Fig. 1 *D*) where the background was uniform and where virions were clearly not in contact with one another. Such images were digitized and the particle orientations were determined by iterative refinement of translational (x, y) and rotational (θ, ϕ, ω) parameters as described previously (Baker et al., 1990; Yeager et al., 1990; Olson et al., 1990). Ninety virion images were extracted from the BPV-1 micrograph and evenly divided into two data sets. We analyzed each set independently and computed two reconstructions, each to 2.5 nm resolution, using those images from each data set (39 from the first and 38 from the second) that displayed the best preservation of particle icosahedral symmetry. The resolution limit of the data was quantitatively assessed by use of a reliability index (R-factor$_{AB}$) that compares both amplitude and phase information between two scaled reconstructions as a function of spatial frequency (Winkelmann et al., 1991). Additional comparisons were made between reconstructions computed from independently refined data sets consisting of either twenty or ten unique virion images each. The final 77-particle BPV-1 reconstruction was generated by adding the 39- and 38-particle three-dimensional density maps together.

For HPV-1, the best 25 virion images (from a total of 68) were combined to compute a three-dimensional reconstruction to 2.5 nm resolution. An R-factor$_{AB}$ comparison of the 25-particle HPV-1 and 77-particle BPV-1 reconstructions was made after the magnification and density of the HPV-1 map were scaled to minimize differences with the BPV-1 map.

All computations were performed on a VAX/VMS 8550 computer (Digital Equipment Corporation, Maynard, MA) with programs written in FORTRAN (Fuller, 1987; Baker et al., 1988, 1989). Digitized micrographs and other images were displayed on a raster graphics device (model 3400; Lexidata Corporation, Billerica, MA) and photo-

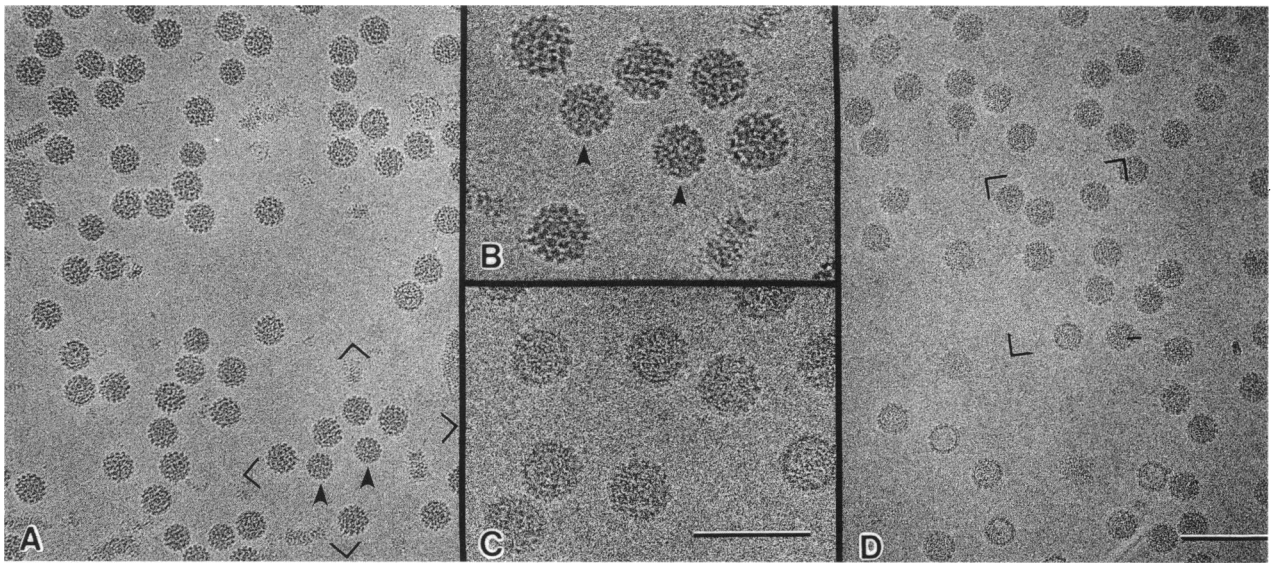

FIGURE 1 Electron micrographs of frozen-hydrated BPV-1 (*A* and *B*), and HPV-1 (*C* and *D*). Boxed regions in *A* and *D* are shown at (2×) higher magnification in *B* and *C*. Arrows in *A* and *B* indicate polyoma virions included in the sample as size markers. *A* and *B* are representative of micrographs recorded at ~1.5 μm underfocus whereas *C* and *D* are typical of those recorded at ~1.0 μm underfocus. Bar = 200 nm (*A* and *D*); 100 nm (*B* and *C*).

graphed with a graphics recorder (model 3000; Matrix Instruments, Orangeburg, NY).

RESULTS

Cryoelectron microscopy

Three-dimensional reconstructions of BPV-1 and HPV-1 were computed from digitized electron micrographs of virions preserved in the frozen-hydrated state. Micrographs were recorded in pairs at two levels of defocus, the first at ~1.0 μm underfocus to recover the maximum structural information and the second at ~1.6 μm underfocus to enhance the contrast of low resolution features (Fig. 1). Visual inspection of such images revealed no significant structural differences between BPV-1 and HPV-1. Both viruses display nearly spherical outer profiles with a highly uniform diameter of ~60 nm. Capsomers are clearly discernable especially at the particle peripheries; they appear coarser and more distinct in BPV-1 and HPV-1 than in comparable images of polyoma virus (Fig. 1, *A* and *B*, *arrows*). The prominent capsomers at the periphery of BPV-1 and HPV-1 have an approximately rectangular profile while en face views of capsomers occasionally give evidence of an axial channel. The projected views of different virions show a diversity of superposition patterns consistent with the idea that virions were randomly oriented in the vitrified field.

Three-dimensional reconstruction

Digitized images of BPV-1 and HPV-1 were analyzed by common-lines and Fourier-Bessel procedures (Crowther, 1971; Fuller, 1987; Baker et al., 1988) to reconstruct the three-dimensional structures of the viruses. A total of 77 virions were included in the BPV-1 reconstruction; 25 were employed for HPV-1. The view directions for all are depicted graphically in Fig. 2. The near-uniform distribution of view orientations for the large number of particle images chosen assured that the three-dimensional density distribution could be calculated with minimal sampling errors to at least 2.5 nm resolution (Crowther et al., 1970*b*). The large size of the data set also provided significant averaging, thus enhancing the signal-to-noise ratio in the reconstruction. The random views enabled features in the three-dimensional structure to be resolved isotropically.

BPV-1 and HPV-1 structures

Solid-surface representations of the BPV-1 and HPV-1 reconstructions (Fig. 3, *A* and *D*, respectively) show that the capsids of both viruses consist of a layer of nearly continuous density (the shell) from which the capsomers project radially. The shell is centered at a radial distance of 22.9 nm and varies in thickness between 1.2 nm and 3.1 nm (Fig. 3, *B*, *C*, *E*, and *F*). It is relatively smooth on

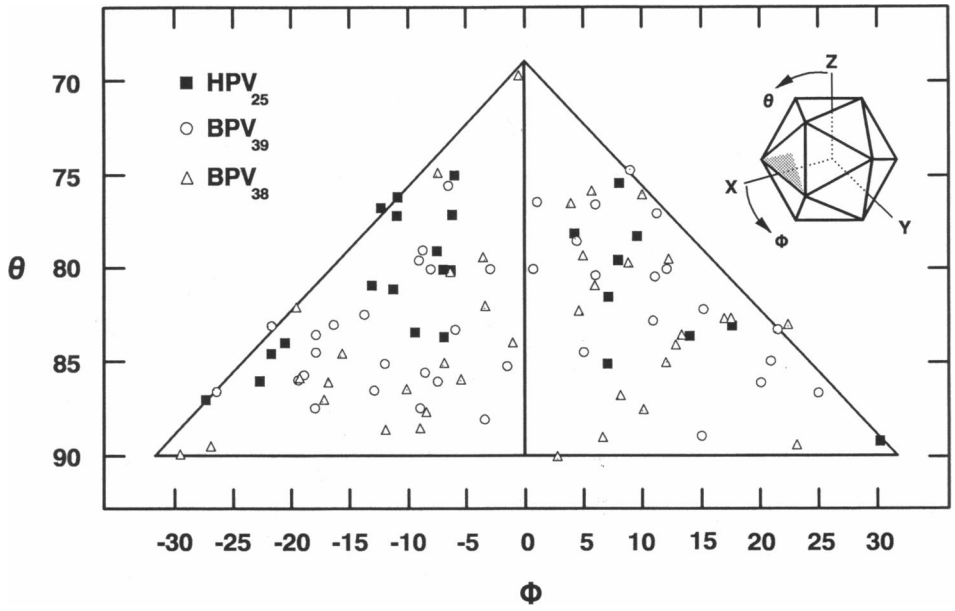

FIGURE 2 Refined orientation angles (θ and ϕ) for the virion images employed to compute the BPV-1 (*open figures*) and HPV-1 (*filled squares*) reconstructions. Open circles and triangles refer to the 39 and 38 particle subsets, respectively, of the BPV-1 data. Orientations are shown as they occur in a single icosahedral asymmetric unit (1/60th of an icosahedron; see *shaded area of inset*) which is bounded by one three-fold (θ = 69°, ϕ = 0°) and two five-fold (θ = 90°; ϕ = −32° and ϕ = +32°) axes.

its inner surface and is separated from the nucleoprotein mass by ~2 nm. Capsomers project to a maximum height of ~5.8 nm above the shell layer. The shell is penetrated by 90 small holes that are <0.5 nm in diameter at the contour level chosen for surface rendering. The holes or very thin regions of the shell occur in rows of three with the central hole in each row coincident with a two-fold axis of symmetry.

In agreement with previous studies of papillomavirus structure (Klug and Finch, 1965; Finch and Klug, 1965; Crowther and Amos, 1972), BPV-1 and HPV-1 are both found to consist of 72 capsomers arranged on a $T = 7$ icosahedral lattice. All capsomers (both hexavalent and pentavalent) have distinct five-fold symmetry suggesting they are pentamers of the major capsid protein, L1 (M_r ~ 55,000). The capsomers consist of a thick trunk region (~8.6 nm in diameter) which extends outward from the shell surface and broadens distally to form a regular five-pointed, star-shaped head. The base of the trunk merges with the shell at a radius of 24.0 nm. The subunits of neighboring capsomers make contact only in the shell layer; at the distal ends they are clearly separated. The center-to-center distance between adjacent 6-capsomers (13.0 nm; measured at the distal ends) is slightly greater than the corresponding spacing between 6- and 5-capsomers (11.9 nm). On its axis each capsomer contains a small depression (more pronounced in HPV-1 than in BPV-1; compare Fig. 3, *A* and *D*) on the external surface and a cylindrical cavity (~2.8 nm in diameter) that extends nearly half way from the interior of the shell to the distal end of the capsomer. The interior openings of capsomer channels can be seen in sectioned views of the capsid shell (Fig. 3, *B* and *E*).

Close-up views of the reconstructions have helped clarify additional aspects of capsomer structure. For example, the protruding (distal) domain of the 5-capsomers appears to occupy a slightly smaller volume than the corresponding region of the 6-capsomers (compare Fig. 4, *A* and *D*). Tip-to-tip and maximum trunk diameter dimensions for BPV-1, respectively, are 10.9 nm and 8.6 nm in the 5-capsomer, but 12.0 nm and 8.9 nm in the 6-capsomer. Both 5-capsomers and 6-capsomers are aligned radially with the capsid icosahedron. Finally, thin (<1.0 nm diameter) projections of density connect the lower side of each 6-capsomer with the nucleoprotein mass at lower radius (Fig. 4, *E* and *F*). Each hexavalent capsomer has five such projections suggesting that one extends from each capsomer subunit. The shape and location of the projections are identical in BPV-1 and HPV-1 indicating that they may represent authentic features even though their dimensions cannot be accurately determined at the nominal resolution (2.5 nm) of the reconstructions.

Comparison of the BPV-1 and HPV-1 reconstructions (Fig. 3, *A* vs *D*, and *B* vs *E*) demonstrates the close morphological similarity in all features of the two capsid

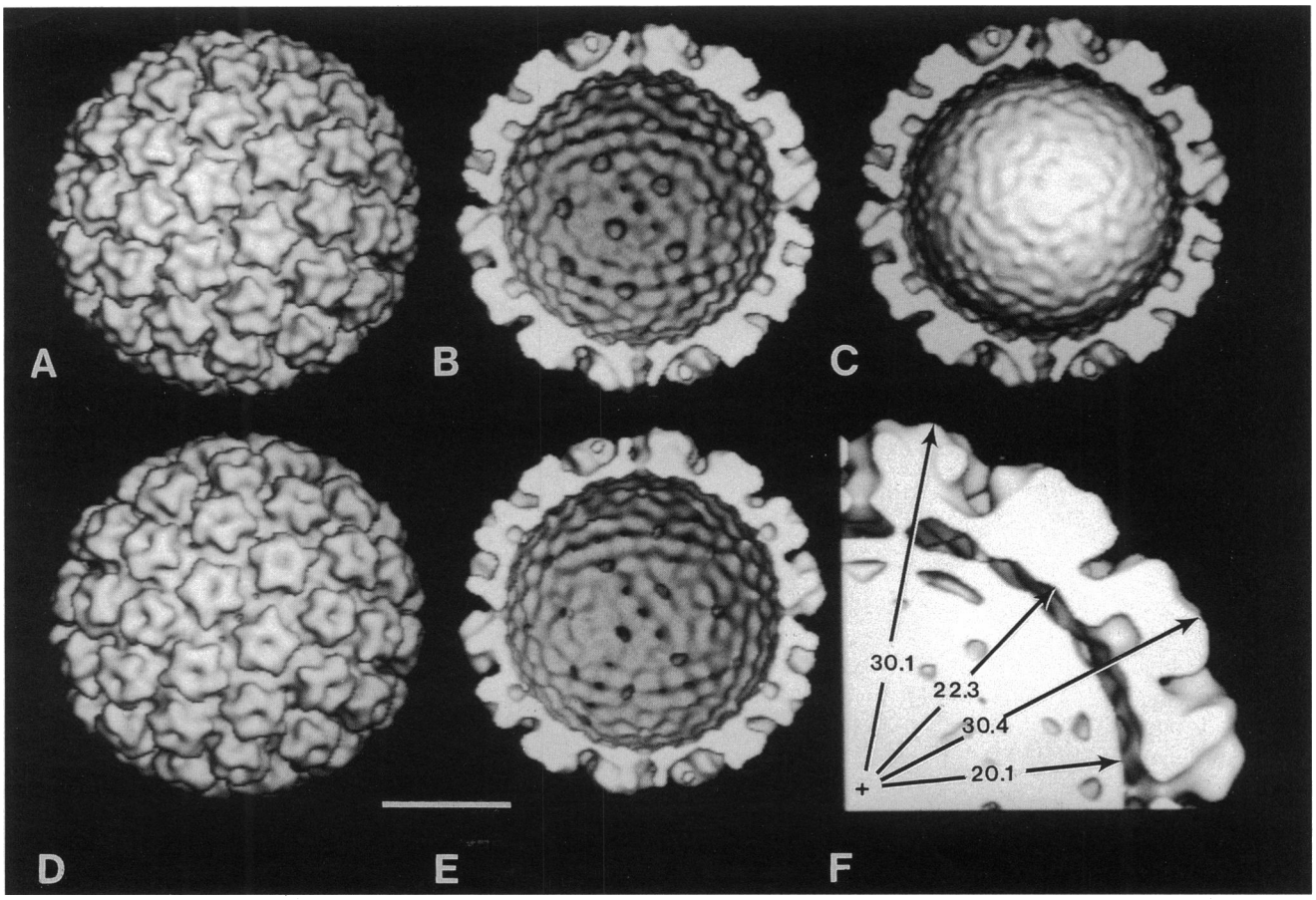

FIGURE 3 Surface shaded (*A*, *D*) and sectioned (*B*, *C*, *E*, *F*) displays of the BPV-1 and HPV-1 reconstructions viewed along a two-fold axis of symmetry. BPV-1 is shown in panels *A–C* and *F*; *D* and *E* show HPV-1. In *B* and *E*, the reconstructions were computationally sectioned at the equator and the nucleoprotein core (all density with $r < 21.0$ nm) was removed. In *C* the BPV-1 capsid shell ($r > 21.0$ nm) was similarly sectioned, but none of the nucleoprotein core was removed. *F* shows an octant of the BPV-1 reconstruction (radii given in nm) which reveals the space (~2 nm) between core and capsid, and the narrow regions of density that connect the two. Bar = 20 nm.

reconstructions. The similarity extends to regions of density barely above the background level and to fine details such as the small openings in the shell layer, the subtle topography of the capsomer surfaces, and the spatial relationships of the star-shaped regions in the capsomer heads. Thus, to the limits of resolution of the two data sets, the BPV-1 and HPV-1 structures can be considered identical. Subsequent discussion will focus on a description of structural features as observed in the 77-particle BPV-1 reconstruction.

Density, presumably corresponding to the viral minichromosome, was observed inside the capsid cavity of both BPV-1 and HPV-1 reconstructions (Figs. 3 *C* and *F*). In both cases, however, the density was smeared and nearly featureless indicating that the nucleoprotein complex is not packaged with the icosahedral symmetry of the capsid. Similarly smeared density was also observed in the nucleohistone core of the SV40 virus reconstruction (Baker et al., 1988; Baker et al., 1989). This does not preclude the possibility that the nucleoprotein may have some symmetric or ordered features that do not have the same (5:3:2) symmetry as the capsid. Alternatively, the nucleosomes within the minichromosome may not be organized in a unique structure and the nucleohistone core may not be packaged the same in all virions.

Quality of the three-dimensional maps

The reliability of the BPV-1 reconstruction was quantified by randomly subdividing the original 90-particle data set and separately processing subsets of 38 and 39 particles to compute independent three-dimensional reconstructions. Inspection showed that the two were indistinguishable in all significant respects. For example,

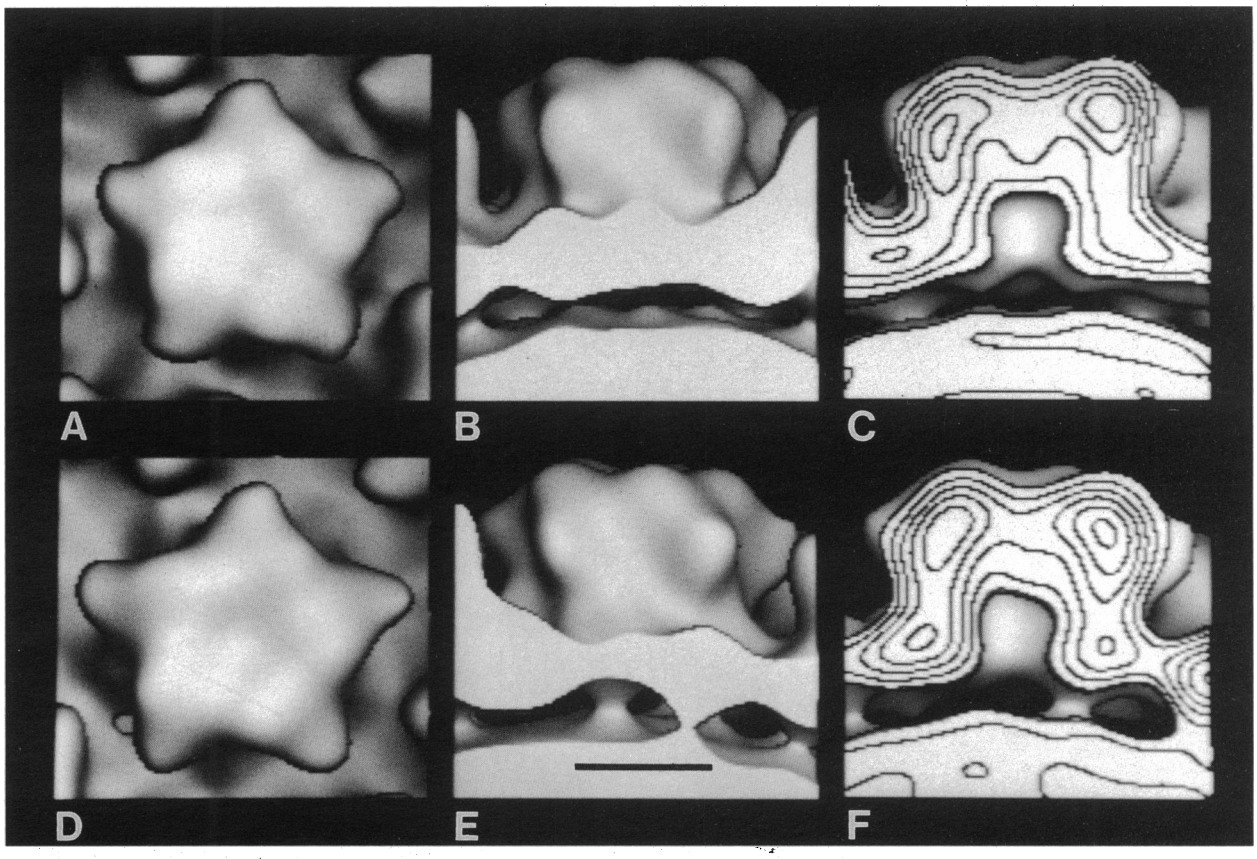

FIGURE 4 Close-up views of the BPV-1 pentavalent (*A–C*) and hexavalent capsomers (*D–F*). Bar = 5 nm.

surface-shaded views (Fig. 5) show that the most subtle features of external architecture, such as capsomer morphology and the positions of lowest density (the trans-shell holes) are remarkably similar in the two reconstructions. The differences that do exist involve regions in which density is about at the level of the noise in the data. Furthermore, these differences are not greater than those found by comparing either partial reconstruction with that derived from the full data set (Fig. 3 *A*). Correspondence between the partial reconstructions provides additional evidence that major BPV-1 structural features are accurately represented in each and in the full 77-particle reconstruction.

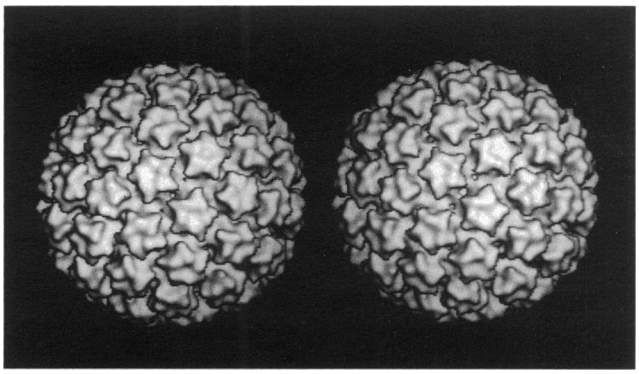

FIGURE 5 Surface-shaded views of reconstructions computed separately from the 39 (*left*) and 38 particle (*right*) subsets of the BPV-1 data. Both reconstructions are viewed along a two fold axis of symmetry.

The quality of the BPV-1 and HPV-1 data were quantitatively tested by computing a reliability index, R-factor$_{AB}$ (Winkelmann et al., 1991), between independent reconstructions (Fig. 6). The results with the large BPV-1 data set clearly indicate that reproducibility improves markedly as the number of virion images increases, especially at higher spatial frequencies near the resolution limit of the data (1/2.5 nm). The trend observed in Fig. 6 implies that additional improvement might be expected if an even larger number of particle images were combined. The downward trend of R-factor$_{AB}$ values might simply reflect the reduction of noise brought about by averaging larger numbers of images.

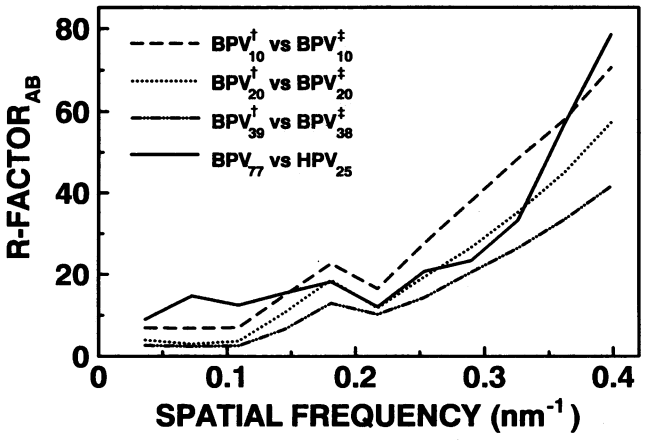

FIGURE 6 R-factor$_{AB}$ comparisons as a function of spatial frequency for four independent pairs of reconstructions. The 77-particle BPV-1 data set was divided at random into two groups (†,‡) and then subdivided into smaller data sets from which three different BPV-BPV comparisons were made (*broken lines*). The reliability of the reconstructions improves significantly, especially at the resolution limits of the data, as the number of particle images included is increased. The solid line compares the final 77-particle BPV-1 and the 25-particle HPV-1 reconstructions.

For hypothetical data consisting of pure noise distributed equally at all spatial frequencies, Fourier transform intensities would be expected to decrease by $N^{1/2}$ when the number of images included in the data set is decreased by the factor N. For such a data set, if the number of images included is increased from 10 to 77 as depicted in Fig. 6, the transform intensitites should decrease by a factor of 2.77 ($=7.7^{1/2}$), which corresponds to a fractional power loss in the transform at all spatial frequencies of 0.64 ($=1.0 - 1.0/N^{1/2}$). For the BPV-1 data, the power loss at 0.4 nm^{-1} (1/2.5 nm) is 0.65, which suggests that the data at this frequency are at the noise level. At slightly smaller spatial frequencies such as 0.33 nm^{-1} (1/3 nm), and 0.28 nm^{-1} (1/3.5 nm) the power losses amount to 0.48 and 0.11, respectively. At 0.25 nm^{-1} (1/4 nm) the power *increases* by 11%. Because R-factor$_{AB}$ values incorporate both amplitude and phase information from the transform (Winkelmann et al., 1991) and thus are not just a measure of amplitude differences as is true for the standard x-ray crystallographic R-factor (see, e.g., Blundell and Johnson, 1976), they provide a more sensitive measure of data agreement. For example, at 0.4 nm^{-1} the average phase difference between the 38- and 39-particle BPV-1 reconstructions is 49.2° whereas it rises to 72.3° for the comparison of two separate 10-particle reconstructions (the global phase differences for these two comparisons are 31.9° and 50.9°, respectively). Thus, at spatial frequencies <0.4 nm^{-1}, the drop in R-factor$_{AB}$ values with larger data sets (Fig. 6) reflects genuine improvement in the reliability of features observed.

Comparison of the 25-particle HPV-1 and the 77-particle BPV-1 reconstructions (*solid line,* Fig. 6) indicates that the two structures are quite comparable at all spatial frequencies depicted in Fig. 6. The differences between BPV-1 and HPV-1 as measured by R-factor$_{AB}$ are at approximately the same level as differences between subsets of the BPV-1 data. Thus, the observed differences between the BPV-1 and HPV-1 structures (Fig. 3) may either represent true morphological differences or they may be caused by fluctuations attributable to the level of noise in the data.

Capsomer subunit morphology

Information about capsomer subunit morphology and about intercapsomer contacts was derived from studies in which the reconstructions were computationally truncated in spherically symmetric shells of progressively decreasing radius. These were examined in surface-shaded representations and also as projected density views (Fig. 7). In surface-shaded views it can be seen that capsomers have clear five-fold symmetry from the tips (r = 29.9 nm) down to the "trunk" region (Fig. 7 *D*; r = 25.0 nm) where the cross-section is more circularly symmetric. At lower radii, five-fold density modulations are again apparent (e.g., Fig. 7 *E*; r = 24.1 nm), but here the capsomer vertices point in different directions than they do in the distal region. This situation is clarified by views of projected density (Fig. 8) which show that the approximate center of each capsomer subunit (i.e. the star point) shifts progressively in a counterclockwise direction beginning just above the capsid shell (r = 26 nm; top left panel of Fig. 8) and ending just inside it (r = 24 nm; *bottom right* of Fig. 8). The shift or turn is found in all subunits of both 5- and 6-capsomers, it amounts to a total rotation of ~30°, and no further turn is observed at lower (i.e., <24 nm) radius. The skewed paths of each 5-capsomer subunit cause the subunit to pass in front of a subunit from a neighboring 6-capsomer and end on the opposite side from where it began. This can be seen by noting the relative positions of the highest density features in the subunits of the 5-capsomer (i.e., the upper capsomer) in Fig. 8.

Intercapsomer contacts

As intercapsomer contacts occur only in the shell layer, they were most clearly recognized when reconstructions were truncated in the shell (r = 22.7 nm) and viewed in projection. Such representations (Fig. 7 *I*) show that 5- and 6-capsomers have quite different morphologies inside the shell. Whereas subunits of the 6-capsomers

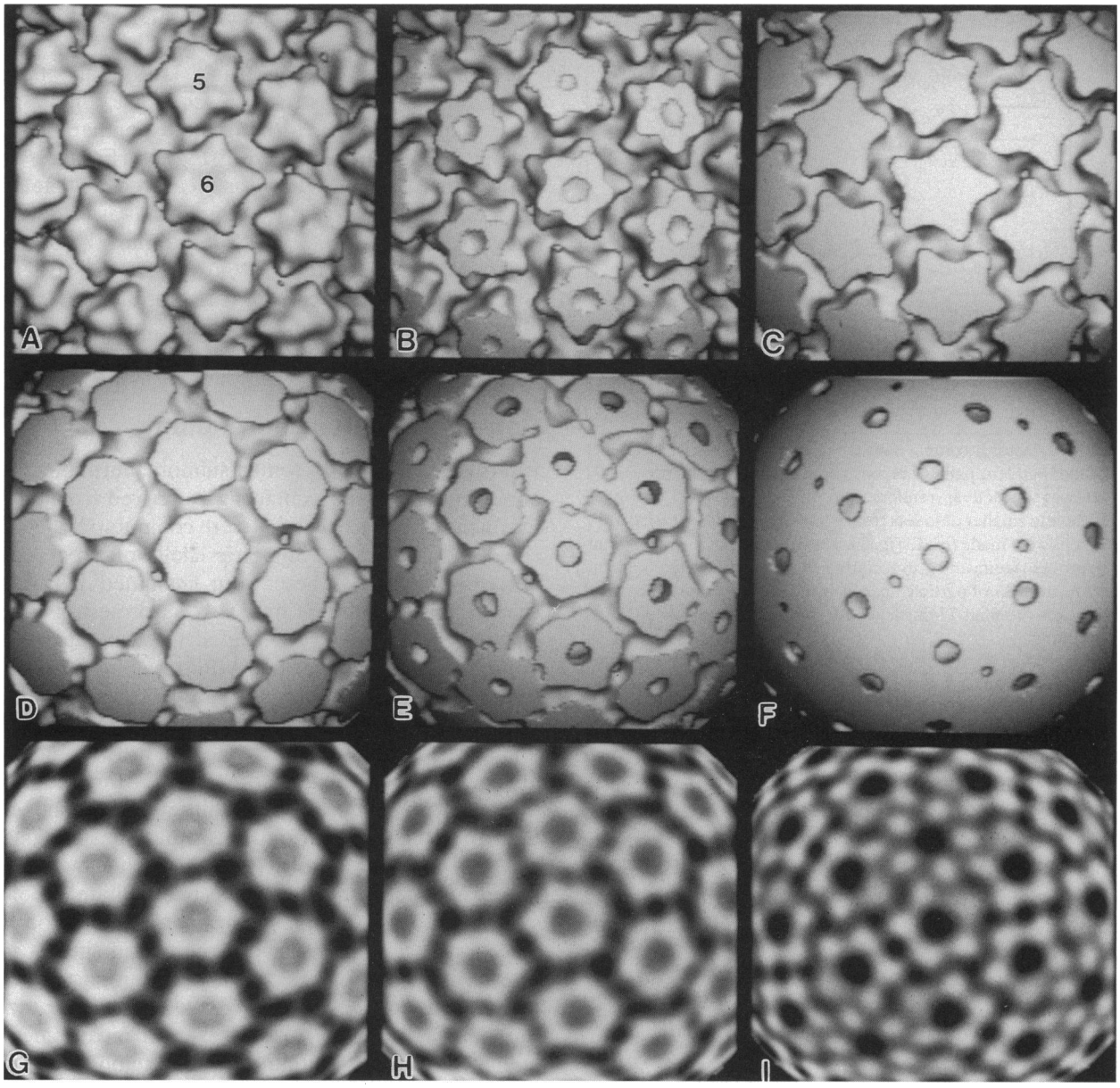

FIGURE 7 The BPV-1 reconstruction represented as surface-shaded views truncated at progressively lower radii (*A–F*) and as projected views of the density at specific radii (*G–I*). Radii of the views are as follows: $A = \infty$ (nothing removed); B = 28.8 nm (capsomer tips removed; distal depression visible on capsomers); C = 27.0 nm (at center of star points); D, G = 25.0 nm (cut at capsomer trunk region where five-fold capsomer symmetry is weak); E, H =24.1 nm (just above capsid shell); F, I = 22.7 nm (at peak of density inside shell layer). The 6-capsomer (labeled "6") at the center of each panel lies just below a 5-capsomer (labeled "5"). The field of view in each panel is ~37.9 nm square.

make contact with neighboring, intracapsomer subunits at low radii and are nearly aligned with the capsomer axis, 5-capsomer subunits appear separated from each other and project laterally away from the capsomer axis at progressively lower radii. Each 5-capsomer subunit makes contact with one neighboring 6-capsomer. In the 6-capsomers, two of the five subunits (*b* and *c* in Fig. 9 *A*) each contact one neighboring capsomer while three adjacent subunits (*d,e,* and *f* in Fig. 9 *A*) coordinate a total of four capsomers. The geometry of capsomer–capsomer contacts is shown schematically in Fig. 9A while Table 1 lists the intercapsomer subunit contacts identified by inspection of Fig. 7 *I* and adjoining radial sections. As expected, all subunit–subunit contacts involv-

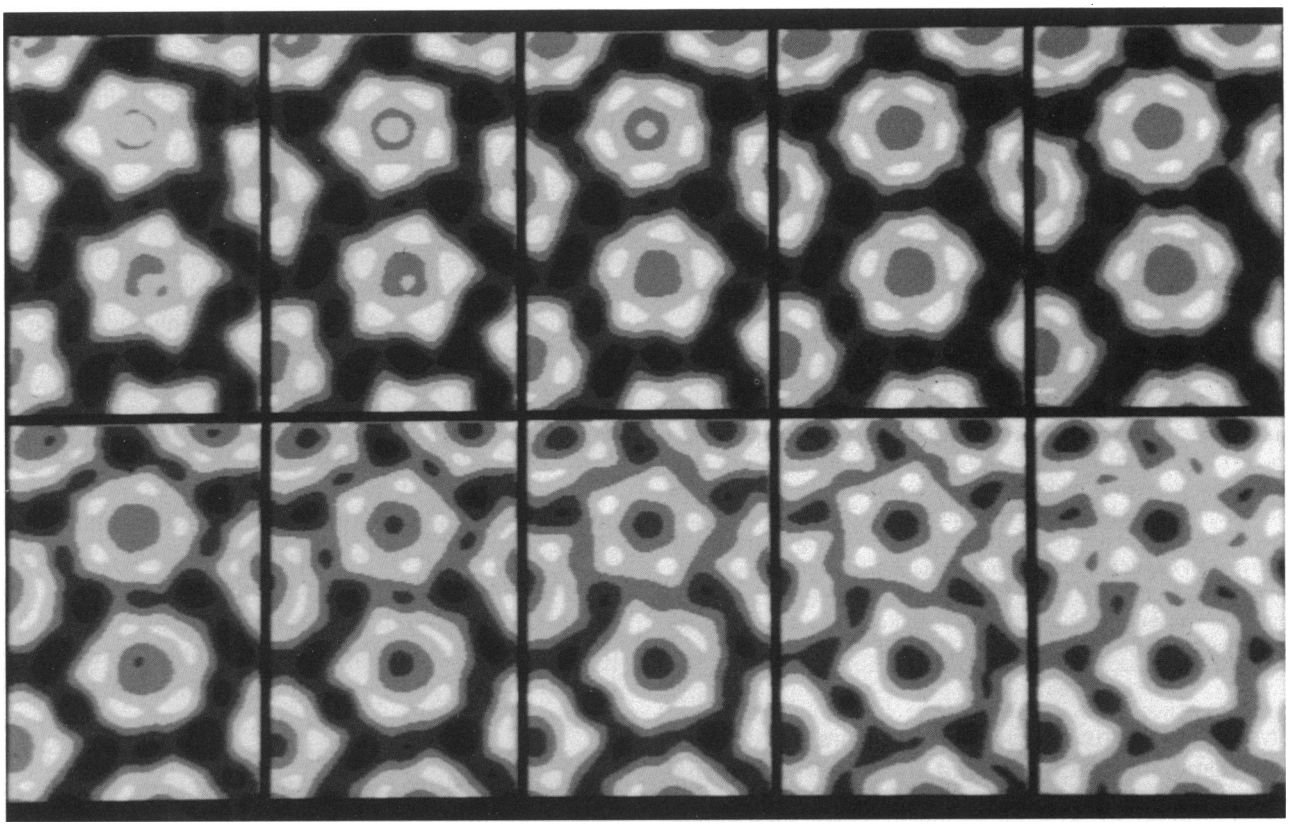

FIGURE 8 Spherical density shells (viewed in projection) of the BPV-1 reconstruction at radii that span the region where capsomer subunits follow a left handed path. Shells are of decreasing radius at 0.24 nm intervals beginning at the upper left (r = 25.5 nm) and ending at the lower right (r = 23.4 nm). One complete 5-capsomer (*upper*) and one complete 6-capsomer (*lower*) is displayed in each panel. Note how the highest density feature in each capsomer subunit traces a counterclockwise trajectory as the radius is decreased and how each 5-capsomer subunit crosses past the closest subunit in the neighboring 6-capsomer.

ing 5-capsomers are found to be identical. Three-way contacts involving subunits c_E-e_D-f_6 and f_D-e_6-c_C are related by an icosahedral two-fold axis of symmetry while subunits d_6, d_B, and d_C are related by a three-fold axis. Intercapsomer contacts in BPV-1 were indistinguishable from those found in HPV-1, but quite different from the contacts reported (Salunke et al., 1989) for polyoma virus (Fig. 9 *B*).

Projections of density at particular radii also showed that capsomers appear to be connected by thin strands of density on the outermost surface of the shell layer (Figs. 7 *G* and *H*). Strands are <1.5 nm in diameter and ten appear to originate from each capsomer. Two connect 5-capsomers to each of their five neighbors whereas in 6-capsomers four neighbors are connected by two strands and two by one strand each. The two joined by one strand are found at either side of the 5-capsomer in the ring of six capsomers that surround each 6-capsomer (i.e., capsomers *E* and *A* in Fig. 9 *A*). Yabe et al. (1979) observed similar intercapsomeric strands in negatively-stained preparatio ns of HPV.

DISCUSSION

The issue of papillomavirus capsomer symmetry is unambiguously resolved by the reconstructions described here. Both pentavalent and hexavalent capsomers of BPV-1 and HPV-1 were found to have five-fold axial symmetry and are therefore most likely to be pentamers of the major capsid protein (L1). Thus, "all-pentamer" capsids have now been reported for members of both genera (papova and papilloma) of the papovavirus family (Rayment et al., 1982; Baker et al., 1988). Despite the conservation of five-fold capsomer symmetry in both genera, the morphology in the projecting domain of the capsomer is the most obvious difference between papilloma and polyoma virus capsid structures. Whereas

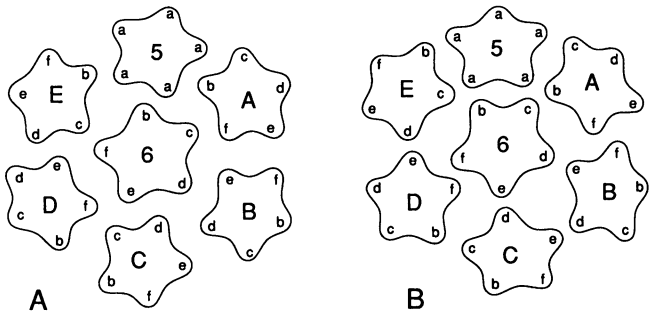

FIGURE 9 Schematic representation of the intercapsomer contacts in the shell layer (r = 22.7 nm) of BPV-1 and HPV-1 (A). For comparison, B shows the intercapsomer contacts as they occur in the contact region (r = 19.0 nm) of the T = 7 shells assembled in vitro from purified polyoma virus major capsid protein (Salunke et al., 1989). Pentavalent (5) and hexavalent (6) capsomers are shown in each case and capsomer subunits are identified by a convention applicable to both types of capsids. Note the quite different geometry of intercapsomer contacts in BPV-1/HPV-1 compared to polyoma virus. To emphasize packing relations, papilloma and polyoma capsomers are depicted at the same size.

polyoma and SV40 capsomers are approximately cylindrical in shape, those of BPV-1 and HPV-1 have additional mass projecting laterally from each subunit to create the star-shaped morphology. The lateral projections probably make papillomavirus capsomers appear larger and more distinct than those of polyoma and SV40 in electron micrographs (Fig. 1). The projections also suggest themselves as sites for the additional mass found in the major capsid proteins of papillomaviruses (M_r ~ 55,000) compared to polyoma and SV40 (M_r ~ 42,000). The BPV-1 and HPV-1 reconstructions gave no clue about the location of the minor capsid protein, L2 (MW ~ 50,000), which accounts for 2–5% of the total BPV-1/HPV-1 protein (Favre et al., 1975).

Capsomer morphology in the projecting domain, as described above, is consistent with and reinforces currently accepted views of papovavirus taxonomy. Whereas all papovaviruses are found to have "all-pentamer" capsids, the distinction between cylindrical and star-shaped capsomers correlates with division of the family into polyoma and papilloma genera. It will now be of interest to have information about capsomer morphology in additional papovaviruses of both genera.

A matter of continuing concern regarding the structures of papovavirus capsids has been to understand how 6-capsomers can coordinate six neighboring capsomers despite the fact that they contain only five subunits. Clearly, not all intercapsomer contacts can be identical. This issue was first raised by results with polyoma virus (Rayment et al., 1982) and later with SV40 (Baker et al., 1988, 1989), but the current study shows that it applies to BPV-1 and HPV-1 as well. Examination of the BPV-1 and HPV-1 reconstructions in the capsid shell layer has shown in a general way how hexavalency is accomplished. The key appears to be the ability of three neighboring subunits (*d,e,* and *f*) of each hexavalent pentamer to coordinate four neighboring capsomers (called *B,C,D,* and *E* in Fig. 9 *A*). The remaining two subunits of the 6-capsomer (i.e., *b* and *c*) each contact one neighboring capsomer. Overall, therefore, the 6-capsomer is able to coordinate a total of six capsomers.

A quite different geometry (Fig. 9 *B*) has been reported for intercapsomer contacts involving hexavalent pentamers in the T = 7 shells isolated from polyoma virus-infected cells (Rayment et al., 1982) or from purified polyoma virus major capsid protein assembled in vitro (Salunke et al., 1989). Here each 6-capsomer makes a nearly perfect face-to-face contact with its neighboring 5-capsomer. 6-capsomer subunits *b* and *c* together coordinate three neighboring capsomers (*E,* 5, and *A* in Fig. 9 *B*) whereas the remaining three subunits (*d,e,* and *f*) bind one capsomer each. The geometry of the intercapsomer contacts as described here makes no specific prediction about the nature of the interatomic forces that underlie them. These could be more similar

TABLE 1 Capsomer subunit contacts in papilloma (BPV-1HPV-1) and polyoma viruses*

	Papilloma		Polyoma	
Subunit(capsomer)	Subunit contact(s)	Capsomer(s) involved	Subunit contact(s)	Capsomer(s) involved
a (Pentavalent)	a_5-b_6	6	a_5-b_6;a_5-c_6	6
b (Hexavalent)	b_6-a_5	5	b_6-c_E;b_6-a_5	*E*; 5
c (Hexavalent)	c_6-f_A	*A*	c_6-a_5;c_6-b_A	5; *A*
d (Hexavalent)	d_6-e_B;d_6-d_B;d_6-d_C	*B; C*	d_6-e_B	*B*
e (Hexavalent)	e_6-c_C;e_6-d_C;e_6-f_D	*C; D*	e_6-d_C	*C*
f (Hexavalent)	f_6-e_D; f_6-c_E	*D; E*	f_6-f_D	*D*

*Capsomer subunits are identified by the system of nomenclature shown in Fig. 9. Contacts for papilloma virus are those identified in the present study for BPV-1 and HPV-1. Contacts for polyoma virus are taken from Salunke et al. (1989).

in polyoma and BPV-1/HPV-1 than the very different geometries would suggest.

A similar divergence is found between polyoma and BPV-1/HPV-1 in the pattern of intercapsomer contacts involving the 5-capsomers. Whereas polyoma 5-capsomers contact neighboring 6-capsomers by the face-to-face juxtaposition mentioned above, in BPV-1/HPV-1 the interaction is an overlapped tip-to-tip contact involving the *a* and *b* subunits as shown in Figs. 7 *I* and 9 *A*. Thus, although the papovaviruses have "all-pentamer" capsids, the morphology of the intercapsomer contacts is not conserved. One can conclude that since the time when polyoma and papilloma viruses diverged evolutionarily, the biological forces tending to preserve "all-pentamer" capsids (i.e., intracapsomer contacts) have been more significant than those operating to conserve capsomer–capsomer interactions. This suggests that the nature of the interactions favoring formation of a pentameric aggregate of the major capsid protein may have a greater influence on virus stability (or function) than the particular set of intercapsomer contacts the subunits are able to make.

Although it was expected at the outset of this study that BPV-1 and HPV-1 would have comparable structures, the degree of similarity is nevertheless still quite striking. As shown in Fig. 6, the similarity extends to the highest frequency information available in electron micrographs. Surface-shaded and sectioned views (Fig. 3) of the two reconstructions show identity near the noise level of density and in the subtlest features visible in these representations (e.g., gentle contours on capsomer surfaces and the extent of the points on the star-shaped capsomer head). The most significant differences occur in the slight depressions found on the capsomer axes at the surfaces (deeper in HPV-1 than in BPV-1) and in the openings of capsomer channels on the inside of the capsid shell (wider in BPV-1 than in HPV-1).

The BPV-1 and HPV-1 structures reported here are consistent with the reconstruction of negatively-stained HPV described by Crowther and Amos (1972). Features such as the $T = 7$ capsid symmetry and relative capsomer size are recognizably the same in the two reconstructions. At the time the first HPV reconstruction was computed, it was expected that the capsid subunits of simple, spherical viruses would obey quasi-equivalent bonding relations (Caspar and Klug, 1962) and therefore the 6-capsomers were believed to be hexameric aggregates of the major capsid protein. Interestingly, re-examination of the earlier HPV reconstruction (see Fig. 1 *a* of Crowther and Amos, 1972) reveals that the projecting domains of the 5-and 6-capsomers had similar stain-excluded volumes and some of the 6-capsomers even appeared to have pentagonal profiles (but with no indication of a star-shaped morphology). Appearance of novel features (e.g., capsomer symmetry and morphology) in the present structures is attributable to greater reliability of the high resolution details obtainable in frozen-hydrated compared to negatively-stained specimens (Adrian et al., 1984; Stewart and Vigers, 1986; Chiu, 1986). Dimensions measured here are slightly greater than those reported earlier for negatively-stained virions (Klug and Finch, 1965; Crowther and Amos, 1972). For instance, the difference in capsid diameter is 59.8 nm (frozen-hydrated) compared to 56.0 nm (negative stain). The differences in all cases are within the range expected for frozen-hydrated compared to negatively-stained virions and are most probably due to the fact that frozen-hydrated specimens do not experience the drying-induced shrinkage characteristic of samples prepared by negative staining (Olson and Baker, 1989).

The skewed capsomer subunit structure observed in BPV-1 and HPV-1 capsomer subunits was completely unexpected. No comparable structural feature is observed in polyoma or SV40 viruses (Rayment et al., 1982; Baker et al., 1988; Baker et al., 1989). Because skewing takes place almost entirely in the region just above the shell layer, it is unlikely that twisting of the subunits is directly involved in capsomer–capsomer interactions. It is possible, however, that this adjustment to capsomer orientation is required to position capsomer subunits for optimal intercapsomer contacts in the shell layer of papilloma viruses. The role of the subunit skew may be clarified by studies, currently in progress, of cottontail rabbit papilloma virus (CRPV) whose $T = 7$ capsid is of opposite handedness (*left*) compared to those of BPV-1 and HPV-1 (*right*). It will be of interest to know whether the subunits in CRPV are skewed and, if so, how they may differ from those in BPV-1/HPV-1.

We gratefully acknowledge Chris Crum for advice on papillomavirus purification, Kelly Dryden and Holland Cheng for programs, Heidi Hinkel and Mary Crouch for assistance with photography and David Belnap for magnification calibration measurements.

This work was supported by National Institutes of Health grants GM33050 (T. S. Baker) and GM34036 (J.C. Brown), by an award from the Jeffress Memorial Trust (J.C. Brown), and by a grant from the Lucille P. Markey Charitable Trust that supports the Purdue Center for Macromolecular Structure.

Received for publication 12 April 1991 and in final form 1 August 1991.

REFERENCES

Adrian, M., J. Dubochet, J. Lepault, and A. W. McDowall. 1984. Cryo-electron microscopy of viruses. *Nature (Lond.)*. 308:32–36.

Baker, T. S., and I. Rayment. 1987. Papovaviridae. *In* Animal Virus Structure. M. V. Nermut, and A. C. Steven, editors. Elsevier, Amsterdam. 335–348.

Baker, T. S., D. L. D. Caspar, and W. T. Murakami. 1983. Polyoma virus "hexamer" tubes consist of paired pentamers. *Nature (Lond.).* 303:446–448.

Baker, T. S., J. Drak, and M. Bina. 1988. Reconstruction of the three-dimensional structure of simian virus 40 and visualization of the chromatin core. *Proc. Natl. Acad. Sci. USA.* 85:422–426.

Baker, T. S., J. Drak, and M. Bina. 1989. The capsid of small papova viruses contains 72 pentameric capsomeres: direct evidence from cryo-electron-microscopy of simian virus 40. *Biophys. J.* 55:243–253.

Baker, T. S., W. W. Newcomb, F. P. Booy, J. C. Brown, and A. C. Steven. 1990. Three-dimensional structures of maturable and abortive capsids of equine herpesvirus 1 from cryoelectron microscopy. *J. Virol.* 64:563–573.

Blundell, T. L., and L. N. Johnson. 1976. Protein Crystallography. Academic Press, New York.

Brady, J. N., and N. P. Salzman. 1986. The papovaviruses: general properties of polyoma and SV40. *In* The Papovaviridae Vol. 1. N. P. Salzman, editor. Plenum Publishing Corp., New York. 1–26.

Caspar D. L. D., and A. Klug. 1962. Physical principles in the construction of regular viruses. *Cold Spring Harbor Symp. Quant. Biol.* 27:1–32.

Chiu, W. 1986. Electron microscopy of frozen, hydrated biological specimens. *Annu. Rev. Biophys. Biophys. Chem.* 15:237–257.

Cowsert, L. M., P. Lake, and A. B. Jenson. 1987. Topographical and conformational epitopes of bovine papillomavirus type 1 defined by monoclonal antibodies. *J. Nat. Cancer Inst.* 79:1053–1057.

Cowsert, L. M., W. P. Pilacinski, and A. B. Jenson. 1988. Identification of the bovine papillomavirus L1 gene product using monoclonal antibodies. *Virology.* 165:613–615.

Crowther, R. A. 1971. Procedures for three-dimensional reconstruction of spherical viruses by Fourier synthesis from electron micrographs. *Phil. Trans. R. Soc. Lond. B. Biol. Sci.* 261:221–230.

Crowther, R. A., L. A. Amos, J. T. Finch, D. J. DeRosier, and A. Klug. 1970*a*. Three-dimensional reconstructions of spherical viruses by Fourier synthesis from electron micrographs. *Nature (Lond.).* 226: 421–425.

Crowther, R. A., D. J. DeRosier, and A. Klug. 1970*b*. The reconstruction of a three-dimensional structure from projections and its application to electron microscopy. *Proc. Roy. Soc. Lond. A Math. Phys. Sci.* 317:319–340.

Crowther, R. A., and L. A. Amos. 1972. Three-dimensional image reconstructions of some small spherical viruses. *Cold Spring Harbor Symp. Quant. Biol.* 36:489–494.

Danos, O., M. Katina, and M. Yaniv. 1982. Human papillomavirus 1a complete DNA sequence: a novel type of genomic organization among papovaviridae. *EMBO (Eur. Mol. Biol. Organ.) J.* 1:231–236.

Eisenberg, D. 1982. A problem for the theory of biological structure. *Nature (Lond.).* 295:99–100.

Favre, M., F. Breitburd, O. Croissant, and G. Orth. 1975. Structural polypeptides of rabbit, bovine and human papillomaviruses. *J. Virol.* 15:1239–1247.

Finch, J. T., and A. Klug. 1965. Structure of viruses of the papilloma-polyoma type. III. Structure of rabbit papilloma virus. *J. Mol. Biol.* 13:1–12.

Fuller, S. 1987. The T = 4 envelope of sindbis virus is organized by interactions with a complementary T = 3 capsid. *Cell.* 48:923–934.

Howley, P. M. 1990. Papillomavirinae and their replication. *In* Fields Virology. B. N. Fields, D. M. Knipe, R. M. Chanock, M. S. Hirsch, J. L. Melnick, T. P. Monath, and B. Roizman, editors. Raven Press, New York. 1625–1650.

Klug, A., and J. T. Finch. 1965. Structure of viruses of the papilloma-polyoma type I: Human wart virus. *J. Mol. Biol.* 11:403–423.

Klug, A. 1983. Architectural design of spherical viruses. *Nature (Lond.).* 303:378–379.

Lancaster, W. D., and C. Olson. 1978. Demonstration of two distinct classes of bovine papilloma virus. *Virology.* 89:372–379.

Newcomb, W. W., and J. C. Brown. 1988. Use of Ar^+ plasma etching to localize structural proteins in viruses: studies with adenovirus 2. *Anal. Biochem.* 169:279–286.

Olson, N. H., and T. S. Baker. 1989. Magnification calibration and the determination of spherical virus diameters using cryo-microscopy. *Ultramicroscopy.* 30:281–298.

Olson, N. H., T. S. Baker, J. E. Johnson and D. A. Hendry. 1990. The three-dimensional structure of frozen-hydrated *Nudaurelia capensis* β virus, a $T = 4$ insect virus. *J. Struct. Biol.* 105:111–122.

Pfister, H. 1987. Papillomaviruses: general description, taxonomy, and classification. In The Papovaviridae, Vol. 2. N. P. Salzman, and P. M. Howley, editors. Plenum Press, New York. 1–38.

Rayment, I., T. S. Baker, D. L. D. Caspar, and W. T. Murakami. 1982. Polyoma virus capsid structure at 22.5Å resolution. *Nature (Lond.).* 295:110–115.

Salunke, D. M., D. L. D. Caspar, and R. L. Garcea. 1986. Self-assembly of purified polyomavirus capsid protein VP1. *Cell.* 46:895–905.

Salunke, D. M., D. L. D. Caspar, and R. L. Garcea. 1989. Polymorphism in the assembly of polyomavirus capsid protein VP1. *Biophys. J.* 56:887–900.

Shah, K. V., and P. M. Howley. 1990. Papillomaviruses. *In* Fields Virology. B. N. Fields, D. M. Knipe, R. M. Chanock, M. S. Hirsch, J. L. Melnick, T. P. Monath, and B. Roizman, editors. Raven Press, New York. 1651–1676.

Shah, K. V. 1990. Polyomaviruses. *In* Fields Virology. B. N. Fields, D. M. Knipe, R. M. Chanock, M. S. Hirsch, J. L. Melnick, T. P. Monath, and B. Roizman, editors. Raven Press, New York. 1609–1623.

Stewart, M., and G. Vigers. 1986. Electron microscopy of frozen-hydrated biological material. *Nature (Lond.).* 319:631–636.

Walker, D. L., and R. J. Frisque. 1986. The biology and molecular biology of JC virus. *In* The Papovaviridae Vol. 1. N. P. Salzman, editor. Plenum Press, New York. 327–377.

Winkelmann, D. A., T. S. Baker, and I. Rayment. 1991. Three-dimensional structure of myosin subfragment-1 from electron microscopy of sectioned crystals. *J. Cell Biol.* 114:701–713.

Yabe, Y., H. Sadakane, and H. Isono. 1979. Connection between capsomeres in human papilloma virus. *Virology.* 96:547–552.

Yeager, M., K. A. Dryden, N. H. Olson, H. B. Greenberg, and T. S. Baker. 1990. Three dimensional structure of rhesus rotavirus by cryoelectron microscopy and image reconstruction. *J. Cell Biol.* 110:2133–2144.